

# Image estimation accounting for point-spread function depth variation in three-dimensional fluorescence microscopy

Chrysanthe Preza<sup>a</sup> and José-Angel Conchello<sup>b</sup>

<sup>a</sup>Department of Electrical Engineering, Washington University, St. Louis, USA

<sup>b</sup>Department of Anatomy and Neurobiology, Washington University, St. Louis, USA

## ABSTRACT

An approximate model for optical-sectioning microscopy describing depth-varying imaging is developed. The model incorporates changes in the point-spread function due to refractive index mismatch between the immersion medium and the specimen, which causes spherical aberration that worsens with increasing depth under the coverslip. Comparison of model predictions to measured images from a bead phantom shows that the approximate model captures the main features in the data. The model presented in this paper is the first step towards depth-variant image estimation for optical-sectioning microscopy. An expectation maximization algorithm for maximum-likelihood restoration based on this model is also presented.

**Keywords:** 3D microscopy, depth-variant imaging model, maximum likelihood estimation

## 1. INTRODUCTION

In three-dimensional (3D) fluorescence microscopy via the method of computational optical sectioning, resolution and contrast of 3D images obtained with a widefield microscope are improved by computational processing. Several different model-based algorithms have been developed for the necessary processing. One thing that all these algorithms have in common is that they are based on a spatially-invariant imaging model which assumes that changes in the point-spread function (PSF) are negligible throughout the volume being imaged. Although this assumption has been necessary in order to keep the computational load practical, it is known that it does not hold for three-dimensional microscopy. Imaging with a fluorescence microscope is spatially variant due to variations in the specimen's refractive index<sup>1</sup> and also due to the imaging depth.<sup>2</sup> In this paper we assume that the specimen has an average uniform refractive index and we study the imaging variations due to depth within the specimen.

Microscope objectives are designed to be aberration-free only when used under the conditions for which they were designed.<sup>2</sup> Typically, they require the specimen to be immediately underneath the coverslip. This condition obviously does not hold for 3D microscopy where only the top-most layer of the specimen is immediately beneath the coverslip. If the specimen is thin, assuming space-invariance may still be a safe assumption. However, typical specimen mounting media, such as water and saline, have a refractive index close to that of water ( $n_w = 1.33$ ) which is different from the refractive index of the objective lens' immersion medium ( $n_a = 1.0$  for air and  $n_o = 1.515$  for oil). This refractive index mismatch causes spherical aberration that worsens with increasing depth under the coverslip.<sup>2-5</sup> Although some microscope objectives can be adjusted to eliminate spherical aberration at planes deeper under the coverslip, they are aberration-free only for the depth for which they were adjusted. Thus, portions of the specimen above and below this depth are imaged with a spherically-aberrant PSF. More recently, methods have been developed that dynamically compensate for the depth-induced spherical aberrations as the microscope is focused at different depths.<sup>6</sup> These methods are based on using deformable mirrors to counteract the phase error caused by the depth under the coverslip. At this time, however, such methods are at experimental stages and not yet commercially available.

---

Further author information:(Send correspondence to C.P.)

C.P.: E-mail: preza@ee.wustl.edu, Telephone: 1 314 935 7340, Address: Washington University, Box 1127, St. Louis, Missouri 63130, USA

J.A.C.: E-mail: josec@3Dmicroscopy.wustl.edu, Telephone: 1 314 362 2940, Address: Washington University School of Medicine, St. Louis, Missouri 63110, USA

Because of this depth-dependence of the PSF, computational-optical sectioning microscopy (COSM) algorithms based on a space-invariant PSF cannot fully compensate for the image degradation introduced by the objective lens. As COSM algorithms increasingly gain acceptance, more will be demanded from them. If quantitative information is needed, such as in fluorescence ratio imaging, results are likely to be in error. To address this problem, it is necessary to incorporate a space varying PSF into COSM algorithms in a way that keeps the computational load tractable. Thus, new algorithms based on a depth-variant imaging model must be developed.

In this paper we present a model that describes depth-variant imaging due to the change of the PSF with increasing imaging depth. In the presentation here we assume that the PSF changes only with depth. The method presented here can be applied to different fluorescence microscope modalities such as wide-field, confocal scanning, etc.

The paper is organized as follows. In Section 2 a model for depth-varying image formation for fluorescence microscopy is presented. In Section 3 simulations and results for the evaluation of the model are presented. A restoration algorithm based on this model is developed in Section 4. The paper concludes with a summary in Section 5.

## 2. DEPTH-VARIANT IMAGING MODEL

For a 3D PSF that varies only with the depth  $z_i$  at which the microscope is focused, the image recorded at  $\mathbf{x}_i \in I$  can be represented by the superposition integral

$$g(\mathbf{x}_i) = \int_O h(\mathbf{r}_i - \mathbf{r}_o, z_i, z_o) s(\mathbf{x}_o) d\mathbf{x}_o. \quad (1)$$

where  $\mathbf{x}_i = (x_i, y_i, z_i)$  and  $\mathbf{r}_i = (x_i, y_i)$  are a 3D and a 2D point, respectively, in image space  $I$ ;  $\mathbf{x}_o = (x_o, y_o, z_o)$  and  $\mathbf{r}_o = (x_o, y_o)$  are a 3D and a 2D point, respectively, in object space  $O$ ;  $h(\mathbf{r}_i - \mathbf{r}_o, z_i, z_o)$  is the depth-varying PSF i.e. the intensity of light at pixel  $\mathbf{r}_i$  produced by an incoherent point source at  $(\mathbf{r}_o, z_o)$  when the microscope is focused at a plane conjugate to  $z_i$ ; and  $s(\mathbf{x}_o)$  is the specimen function, i.e. the concentration of fluorescent dye at  $\mathbf{x}_o \in O$ .

In a restoration algorithm, Equation (1) is evaluated in discrete form to yield an estimated sampled image. Numerical evaluation of Equation (1) requires storing a 4D array  $h(\mathbf{r}_o, z_i, z_o)$  because a different PSF is needed for each plane in the image. Additionally, the evaluation of a large number of 2D convolutions (one convolution for each pair of depths  $(z_i, z_o)$ ) is required. A reduction of the number of PSFs needed to evaluate Equation (1) can be made by allowing a variable number of neighboring pixels to be associated with the same PSF.<sup>7</sup> If the PSF does not change very rapidly with depth  $z_i$ , then it is possible to approximate Equation (1) using a small number of PSFs, each computed at a different depth  $z_i = Z_m$ ,  $m = 1, 2, 3, \dots, M$ . This approximation is similar to the one proposed by Trussell and Hunt<sup>8</sup> and used by Boden, et al. for astronomical imaging.<sup>9</sup>

In our approach, we partition the object space  $O$  into  $M$  non-overlapping strata, centered at depths  $z_i = Z_m$ :

$$O_m = \{\mathbf{r}_o, z_o : Z_m - \frac{t_m}{2} \leq z_o < Z_m + \frac{t_m}{2}\}; \quad m = 1, 2, 3, \dots, M$$

where  $t_m$  is the width of each stratum and it is equal to the distance between two consecutive depths  $z_i = Z_m$  along the  $z$ -axis.  $t_m$  is chosen such that the PSF varies little from one depth to the next. The object can be considered as the superposition of these strata and can be written as

$$\begin{aligned} s(\mathbf{x}_o) &= \sum_{m=1}^M s_m(\mathbf{x}_o), \quad \text{where} \\ s_m(\mathbf{x}_o) &= s(\mathbf{x}_o) \text{rect}[(z_o - Z_m)/t_m], \quad \text{and} \\ \text{rect}(z) &= \begin{cases} 1 & \text{if } |z| \leq 1/2 \\ 0 & \text{otherwise.} \end{cases} \end{aligned} \quad (2)$$

Using Equation (3), Equation (1) can be rewritten as

$$g(\mathbf{x}_i) = \sum_{i=1}^M \int_{O_m} h(\mathbf{r}_i - \mathbf{r}_o, z_i, z_o) s_m(\mathbf{x}_o) d\mathbf{x}_o. \quad (3)$$

Because we have assumed that the PSF does not change significantly within a stratum the superposition integral in Equation (3) can be approximated by the convolution of the PSF at depth  $z_i = Z_m$ , the center of the stratum, and the corresponding stratum of the object. Thus, if we define a sequence of  $M$  PSF's at depths  $z_i = Z_m$  as

$$h_m(\mathbf{x}_o) = h(\mathbf{r}_o, Z_m, z_o) \quad m = 1, 2, 3, \dots, M \quad (4)$$

and a sequence of images

$$g_m(\mathbf{x}_i) = \int_{O_m} h_m(\mathbf{x}_i - \mathbf{x}_o) s_m(\mathbf{x}_o) d\mathbf{x}_o, \quad (5)$$

then Equation (3) can be approximated by

$$g(\mathbf{x}_i) \approx \sum_{i=1}^M g_m(\mathbf{x}_i). \quad (6)$$

Thus, the depth-varying model can be approximated by the superposition of all the strata images.

### 3. MODEL EVALUATION

#### 3.1. Methods

##### 3.1.1. Synthetic data

To evaluate the imaging model, synthetic images were generated using the approximate depth-variant model (Eq. 6) for three numerically-generated test objects. Each stratum in the approximation had 5 planes. Point-spread functions of a 60x1.4 N.A. oil-immersion objective lens at different depths were computed with the PSF program in the XCOSM v2.5 package<sup>10</sup> for a fluorescent wavelength equal to 530 nm. In all cases it was assumed that zero depth coincides with the location of the cover slip.

The first test object consists of three small spheres (0.45  $\mu m$  in diameter) positioned at depths 0.0  $\mu m$ , 0.9  $\mu m$ , and 1.8  $\mu m$  in a  $128 \times 128 \times 128$  pixel volume with cubic pixels of size 0.09  $\mu m^3$ . The distance between the spheres is 0.54  $\mu m$ . Test objects with a single sphere at the indicated depths were also generated. For the model predictions 5 PSFs were generated at depths of 0.45  $\mu m$  apart. The spheres were centered in each plane of the 3D image and it was assumed that the average refractive index of the object is equal to 1.33.

The third test object consists of a 4  $\mu m$  in diameter sphere positioned at zero depth in a  $256 \times 256 \times 256$  pixel volume with cubic pixels of size 0.06  $\mu m^3$ . It was assumed that the average refractive index of the object is equal to 1.4. For the model predictions 14 PSFs were generated at depths of 0.3  $\mu m$  apart.

For comparison, synthetic images of the test objects were also computed using the space-invariant imaging model for COSM which is the 3-D convolution of the object with the PSF defined at zero depth.

##### 3.1.2. Measured data

An image of a 4  $\mu m$  in diameter bead phantom was measured with a Nikon Eclipse TE200 equipped with a charged-couple device camera (Photometrics Quantix 57, Roper Scientific) with  $535 \times 512$  pixels and well size equal to 13  $\mu m \times 13 \mu m$ . We used an infinity corrected Plan Apo 60x1.4 N.A. oil-immersion DIC H objective lens with working distance equal to 0.21  $\mu m$  and a  $2 \times$  relay lens yielding an effective pixel of 0.12  $\mu m$  in the image. The refractive index of the oil used is 1.5150. Excitation and emission filters centered at 490 nm and 530 nm with full-width at half maximum of 20 nm and 30 nm respectively were used. The bead, stained with four different fluorescent dyes, was mounted in an optical cement with refractive index  $n = 1.4$  (TetraSpec Kit T-14792, Molecular Probes, Inc).

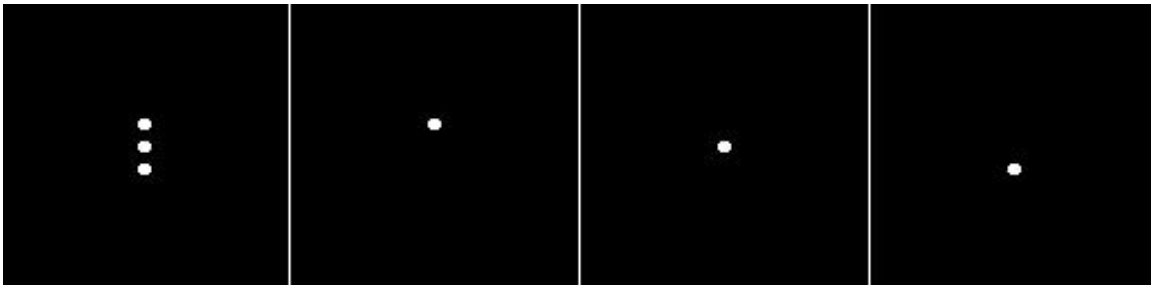


**Figure 1.**  $xz$ -section images through the center of the 3-sphere object (leftmost image) and of objects with a single sphere at depths:  $0 \mu m$ ,  $0.9 \mu m$ , and  $1.8 \mu m$  from left to right.

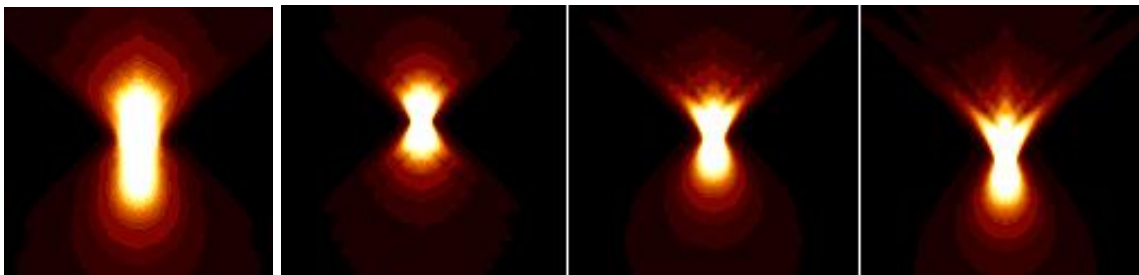


**Figure 2.**  $xz$ -section images through the center of: the superposition image obtained by adding the three images of objects with a single sphere (leftmost image) and the images of objects with a single sphere at depths:  $0 \mu m$ ,  $0.9 \mu m$ , and  $1.8 \mu m$  from left to right. The intensity in the brighter parts of the image is intentionally saturated in order to reveal detail in the low-intensity portions of the image.

### 3.2. Results

We first demonstrate the effect of the changing PSF on the imaging process and the strata concept utilized in the depth-variant imaging model. Figure 1 shows the 3-sphere object decomposed into three separate objects containing a single sphere. Each sphere is at a different depth and thus imaged by the PSF that corresponds to that depth. The image of each sphere is shown in Figure 2. Note how the images become asymmetrical along  $z$  with increasing depth. The superposition of the three single-sphere object images in Figure 2 (leftmost image) is the image of the 3-sphere object predicted by the depth-variant model (Figure 3).

Model predictions of the 3-sphere phantom obtained with the depth-variant model and the space-invariant model are compared in Figures 3 and 4. The 3 spheres can be resolved in the space-invariant model prediction but not in the depth-variant model prediction demonstrating that blurring due to spherical aberration reduces the resolution in the image.

For the evaluation of the depth-variant imaging model we compare in Figure 5 a measured image of the  $4\text{-}\mu m$  bead phantom (see Section 3.1.2) to a model prediction generated as described in Section 3.1.1. Profiles along  $z$  through the center of the images are plotted in Figure 6. As evident from these figures the depth-variant model captures the major features in the measured image of the bead.

## 4. RESTORATION ALGORITHM

The Expectation Maximization (EM) algorithm for maximum likelihood estimation based on Poisson statistics derived by Dempster, Laird, and Rubin<sup>11</sup> has been adapted by us and others to optical sectioning microscopy

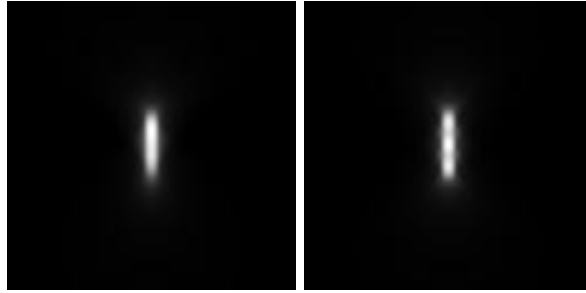


**Figure 3.** Comparison of  $xz$ -section images predicted by the depth-variant (DV) model (left) and the space-invariant (SI) model (right).

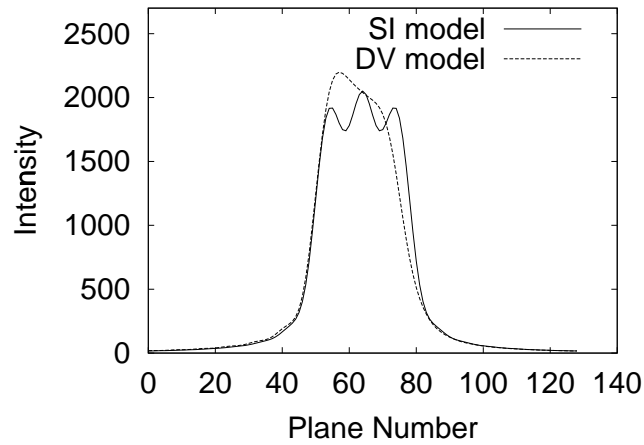


**Figure 4.** Profiles through the  $xz$ -section images of the model predictions of the 3-sphere phantom with the depth-variant model (DV-model) and the space-invariant model (SI-model). Plane zero corresponds to the top of the images in Figure 3.

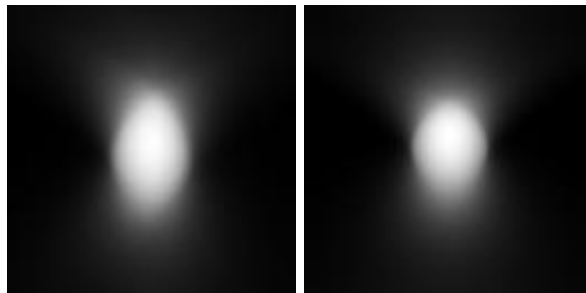


**Figure 5.** Comparison of  $xz$ -section images through the center of a measured image (left) and a synthetic image (right) of the  $4\text{-}\mu\text{m}$  bead phantom.

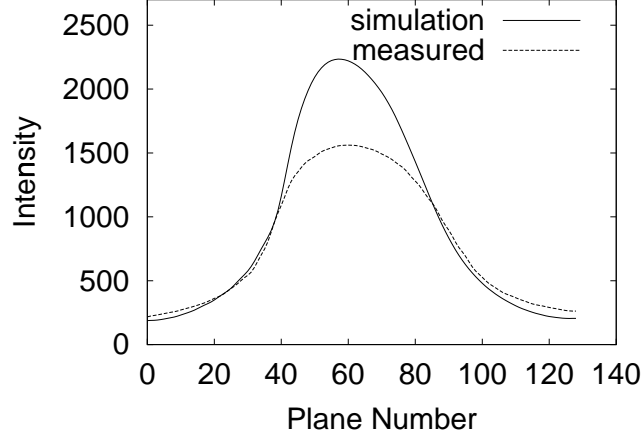


**Figure 6.** Profiles through the  $xz$ -section images of the  $4\text{-}\mu\text{m}$  bead phantom shown in Figure 5. Plane zero corresponds to the top of the images.

for a space-invariant imaging model.<sup>12-17</sup> Using Equation (6) to approximate the depth-variant imaging model we have derived a new EM algorithm for optical sectioning microscopy.

Following the EM formalism,<sup>18</sup> we define the complete data set as  $N(d\mathbf{x}_i, d\mathbf{x}_o)$ , the number of photons emitted from  $[\mathbf{x}_o, \mathbf{x}_o + d\mathbf{x}_o] \in O$  and detected at  $[\mathbf{x}_i, \mathbf{x}_i + d\mathbf{x}_i] \in I$ . For a given pair of points  $(\mathbf{x}_i, \mathbf{x}_o)$ ,  $N(d\mathbf{x}_i, d\mathbf{x}_o)$  follows a Poisson distribution with mean

$$\mu(d\mathbf{x}_i, d\mathbf{x}_o) = h_m(\mathbf{x}_i - \mathbf{x}_o) s_m(\mathbf{x}_o) d\mathbf{x}_i d\mathbf{x}_o \quad \text{for } \mathbf{x}_o \in O_m$$

The log-likelihood of the complete data set is given by

$$L_{\text{cd}} = - \int_I \int_O \mu(d\mathbf{x}_i, d\mathbf{x}_o) + \int_I \int_O \ln[s(\mathbf{x}_o)] N(d\mathbf{x}_i, d\mathbf{x}_o), \quad (7)$$

where terms independent of  $s(\mathbf{x}_o)$  were dropped. The expectation of Equation (7) conditioned on the estimate at iteration  $(k)$ ,  $\hat{s}^{(k)}(\mathbf{x}_o)$ , and the recorded data  $g(\mathbf{x}_i)$  modeled by Equation (6) is given by

$$\begin{aligned} Q[s; \hat{s}^{(k)}] &= - \int_O \sum_m s_m(\mathbf{x}_o) \int_I h_m(\mathbf{x}_i - \mathbf{x}_o) d\mathbf{x}_i d\mathbf{x}_o \\ &+ \int_O \ln[s(\mathbf{x}_o)] \sum_m \hat{s}_m^{(k)}(\mathbf{x}_o) \int_I h_m(\mathbf{x}_i - \mathbf{x}_o) \frac{g(\mathbf{x}_i)}{\hat{g}^{(k)}(\mathbf{x}_i)} d\mathbf{x}_i d\mathbf{x}_o, \end{aligned} \quad (8)$$

where  $\hat{g}^{(k)}(\mathbf{x}_i)$  is the image of the specimen function estimate at iteration  $(k)$ . At each iteration of the EM algorithm an estimate of  $s(\mathbf{x}_o)$  is computed to maximize Equation (8). The maximization defined by

$$\begin{aligned} \hat{s}^{(k)}(\mathbf{x}_o) &= \operatorname{argmax} Q[s; \hat{s}^{(k)}], \\ s(\mathbf{x}_o) &\geq 0 \end{aligned} \quad (9)$$

yields the estimate

$$s_m^{(k+1)}(\mathbf{x}_o) = \frac{1}{H_m} s_m^{(k)}(\mathbf{x}_o) \int_I h_m(\mathbf{x}_i - \mathbf{x}_o) \frac{g(\mathbf{x}_i)}{\hat{g}^{(k)}(\mathbf{x}_i)} d\mathbf{x}_i, \quad (10)$$

for  $m = 1, \dots, M$ , where  $H_m = \int_I h_m(\mathbf{x}_i - \mathbf{x}_o) d\mathbf{x}_i$ .

Equation 10 yields an iterative depth-variant maximum-likelihood image estimation algorithm derived based on an approximate imaging model. The approximation in the imaging model improves as the number of PSFs (or strata) increases. However, increasing the number of strata increases computation time. Thus, the number of strata (Equation (3)) used in the approximation model regulates the trade-off between the computation time and the quality of the estimated specimen function.

## 5. SUMMARY AND CONCLUSIONS

We have developed a new imaging model for computational optical sectioning microscopy that takes into account a depth-variant PSF, i.e. a PSF that changes with imaging depth. Comparison of model predictions with measured images of a simple phantom shows that the model captures the major features in the measured data. Comparison of the new model predictions to images predicted by the conventional (space-invariant) COSM model shows significant differences. These differences suggest that existing COSM restoration algorithms, based on the space-invariant imaging model, cannot fully compensate for the image degradation introduced by the spherical aberration due to imaging depth. To ameliorate this problem we have developed a new restoration method based on the depth-variant imaging model. The new expectation maximization algorithm for maximum-likelihood estimation was presented in the paper. We are currently implementing this algorithm and results from its evaluation will be presented in a future publication.

## 6. ACKNOWLEDGEMENTS

This work was supported by the National Institutes of Health grants RO1 GM55708 and 5R01 GM4979808.

## REFERENCES

1. Z. Kam, B. Hanser, M.G.L. Gustafsson, D. A. Agard, and J.W. Sedat. "Computational adaptive optics for live three-dimensional biological imaging". *Proceedings of the National Academy of Science*, 98(7):3790–3795, 2001.
2. S. F. Gibson and F. Lanni. "Experimental Test of an Analytical Model of Aberration in an Oil-Immersion Objective Lens Used in Three-Dimensional Light Microscopy". *J. Opt. Soc. Am. A*, 9(1):154–66, 1992.
3. S. F. Gibson and F. Lanni. "Measured and analytical point spread functions of the optical microscope for use in 3-D optical serial sectioning microscopy". In *Iptical Microscopy for Biology*. Wiley-Liss, Inc., New York, 1990.
4. H. Leung. "The importance of mounting medium's refractive index and cover glass thickness for reducing optical aberrations on confocal laser scanning microscope (CLSM)". *Microscopical Society of Canada Bulletin*, 21(2):19–24, 1993.
5. J. G. McNally, C. Preza, J.-A. Conchello, and L. J. Thomas, Jr. "Artifacts in Computational Optical-Sectioning Microscopy". *Journal of the Optical Society of America A*, 11(3):1056–1067, 1994.
6. L.R. Sherman, O. Albert, Schmidt C.F., G.V. Vdovin, G.A. Mourou, and T.B. Morris. "Adaptive compensation for aberrations in ultrafast three dimensional microscopy using a deformable mirror". In C. J. Cogswell, J.-A. Conchello, and T. Wilson, editors, *Three-Dimensional and Multidimensional Microscopy: Image Acquisition and Processing VII*, volume Proc. SPIE 3919, pages 9–13, 2000.
7. M. Faisal, A. D. Lanterman, D. L. Snyder, and R. L. White. "Implementation of a modified Richardson-Lusy method for image restoration on a massively parallel computer to compensate for space-variant point spread of a charge-coupled-device camera". *Journal of the Optical Society of America A*, 12(12):2593–2603, 1995.
8. H.J. Trussell and B. R. Hunt. "Image Restoration of Space-Variant Blurs by Sectioned Methods". *IEEE Transactions on Acoustics, Speech, and Signal Processing*, ASSP-26(6):608–609, 1978.
9. A. F. Boden, D. C. Redding, R. J. Hanisch, and J. Mo. "Massively parallel spatially variant maximum-likelihood restoration of Hubble Space Telescope imagery". *Journal of the Optical Society of America A*, 13(7):1537–1545, 1996.
10. The XCOSM deconvolution package is available from URL <http://3Dmicroscopy.wustl.edu/xcosm>.
11. A. D. Dempster, N. M. Laird, and D. B. Rubin. "Maximum Likelihood From Incomplete Data via the EM Algorithm". *J. Royal Statistical Society, B*, 39:1–37, 1977.
12. J.-A. Conchello and E. W. Hansen. "Enhanced 3-D Reconstruction From Confocal Scanning Microscope Images. 1: Deterministic and Maximum Likelihood Reconstructions". *Applied Optics*, 19(26):3795–3804, 1990.
13. J.-A. Conchello and J.G. McNally. "Fast regularization technique for expectation maximization algorithm for computational optical sectioning microscopy". In C. J. Cogswell, G. S. Kino, and T. Wilson, editors, *Proceedings of the IS&T/SPIE symposium on Electronic Imaging, Science and Technology*, volume 2655, pages 199–208, 1996.

14. Markham J. and J.-A. Conchello. "Tradeoffs in regularized maximum-likelihood image restoration". In C. J. Cogswell, J.-A. Conchello, and T. Wilson, editors, *Three-Dimensional Microscopy: Image Acquisition and Processing IV*, volume Proc. SPIE 2984, pages 136–145, 1997.
15. G. M. P. van Kempen, L.J. van Vliet, P.J. Verveer, and H.T.M van der Voort. "A quantitative comparison of image restoration methods for confocal microscopy ". *Journal of Microscopy*, 185:354–365, 1994.
16. T. J. Holmes. "Expectation-maximization Restoration of Band-limited, Truncated Point-Process Intensities with Application in Microscopy". *J. Opt. Soc. Am. A*, 6(7):1006 – 1014, July 1989.
17. S. Joshi and M. I. Miller. "Maximum *a posteriori* Estimation with Good's Roughness for Optical-Sectioning Microscopy". *Journal of the Optical Society of America A*, 10(5), 1993.
18. D.L. Snyder and M. I. Miller. *Random Point Processes in Time and Space*. Springer-Verlag, New York, 1991.